Structural Inheritance Controls Strain Distribution During Early Continental Rifting, Rukwa Rift

Folarin Kolawole[1,2*], Thomas B. Phillips[3], Estella A. Atekwana[4] and Christopher A-L. Jackson[5]
[1]*School of Geosciences, University of Oklahoma, 100 East Boyd Street, RM 710, Norman, Oklahoma 73019*
[2]*Now at BP America, 501 Westlake Park Blvd, Houston, TX 77079*
[3]*Department of Earth Sciences, Durham University, Science Labs, Durham DH1 3LE*
[4]*Department of Earth Science, University of Delaware, 101 Penny Hall, Newark, Delaware 19718*
[5]*Department of Earth and Environmental Sciences, The University of Manchester, Williamson Building, Oxford Road, Manchester, M13 9PL, UK*

*Corresponding Author: F. Kolawole (folarin.kol@gmail.com)

ABSTRACT

Little is known about rift kinematics and strain distribution during the earliest phase of extension due to the deep burial of the pre-rift and earliest rift structures beneath younger, rift-related deposits. Yet, this exact phase of basin development ultimately sets the stage for the location of continental plate divergence and breakup. Here, we investigate the structure and strain distribution in the multiphase Mesozoic-Cenozoic magma-poor Rukwa Rift, East Africa during the earliest phase of extension. We utilize aeromagnetic data that image the Precambrian Chisi Suture Zone (CSZ) and bounding terranes, and interpretations of 2-D seismic reflection data to show that, during the earliest rift phase (Permo-Triassic Karoo): (1) the rift was defined by the Lupa Fault, which exploited colinear basement terrane boundaries, and a prominent intra-basinal fault cluster (329° ±9.6) that trends parallel to and whose location was controlled by the CSZ (326°); (2) extensional strain in the NW section of the rift was accommodated by both the intra-basinal fault cluster and the border fault, where the intra-basinal faulting account for up to 60% of extension; in the SE where the CSZ is absent, strain is primarily focused on the Lupa Fault. The early-rift strain in the Rukwa Rift is thus, not accommodated by distributed faulting as suggested by classic rift models; instead, strain focuses relatively quickly on large faults and intra-basinal fault clusters following pre-existing intra-basement structures; (3) two styles of early-phase strain localization are evident, in which strain is localized onto a narrow discrete zone of basement weakness in the form of a large rift fault (Style-1 localization), and onto a broader discrete zone of basement weakness in the form of a fault cluster (Style-2 localization). We argue that the CSZ and adjacent terrane boundaries represent zones of basement mechanical weakness that controlled the first-order strain distribution and rift development during the earliest phase of extension. The established early-rift structure, modulated by structural inheritance, then persisted through the subsequent phases of rifting. The results of our study, in a young, and relatively well-exposed and data-rich rift, are applicable to understanding the structural evolution of deeper, buried ancient rifts.

Keywords: Continental Rifting, Tectonic Strain, Normal Faults, Rukwa Rift, East African Rift System

INTRODUCTION

Tectonic extension of the continental lithosphere is typically accommodated by the brittle deformation of the upper crust, demonstrated by the emergence of normal fault populations (Cowie et al., 2005; Agostini et al., 2011; Muirhead et al., 2016, 2019). Classic models for the evolution of continental rifts suggest that during the early phase of extension, strain is initially accommodated by the development of distributed normal faults, with strain subsequently localizing onto a few large faults (e.g., Gawthorpe and Leeder, 2000). Strain localisation may be associated with the basinward migration of faulting (e.g., Cowie et al., 2005; Nixon et al., 2016; Naliboff et al., 2017). A comparison of active, early-stage, magma-rich and magma-poor rift segments along the East African Rift System (EARS) show that in contrast to the magma-rich rift basins where strain is accommodated by both the large basin-bounding faults (border faults) and intra-basinal faults, the border faults accommodate most (~90 %) of the strain in the magma-poor rift segment (Muirhead et al., 2019). Elsewhere along the EARS, the incipient (<3 Ma) magma-poor Zomba Graben, southern Malawi Rift, has already witnessed the localization of strain in the rift axis, with the related faults presently accounting for up to 55 % (±24) of the extensional strain (Wedmore et al., 2020). The evidence presented in these studies indicate that early-phase extensional strain along magma-poor continental rifts may or may not be primarily accommodated by the border faults. Thus, there is a need to better understand other mechanisms that can facilitate early focusing of intra-basinal faulting and extensional strain in magma-poor continental rifts.

Since continental rifts typically rupture previously deformed lithosphere (Wilson, 1966; Dewey and Spall,1975; Buiter and Torsvik, 2014), the distribution of early-phase strain in magma-poor rifts can be complex due to the interaction between faults that exploit or reactivate pre-existing structures, and those that form independently of any pre-existing structure (e.g., Manatschal et al., 2015; Kolawole et al., 2018; Ragon et al., 2019; Schiffer et al., 2019; Phillips et al., 2019a,b; Heilman et al., 2019; Osagiede et al., 2020). Overall, very little is known about the earliest phase of continental extension, and even less of how strain is partitioned along inherited structures; this reflects the fact that the associated structures and related stratigraphic record are typically deeply buried beneath younger (i.e., post-rift or later rift phase) sequences and are thus difficult to image with geophysical data, or are overprinted by later tectonic events (e.g., post-rift plate collision). This knowledge gap limits a fuller understanding of the spectrum of processes that govern continental rifting and breakup in space and time.

The EARS (Fig. 1A) is the largest active continental rift system on Earth. This system, which formed by the stretching of previously deformed lithosphere, is characterized by segments that span the major stages of continental rifting from inception to transitional crust (e.g., Daly, 1989; Delvaux, 2001; Chorowicz, 2005). We integrate available geophysical and geological datasets from the multiphase magma-poor Rukwa Rift (Figs. 1A-B, 2A-D) to explore how strain was distributed during the earliest phase of extension, and investigate the dominant controls. We show that the lithosphere-scale Precambrian Chisi Suture Zone (CSZ) that extends beneath the Rukwa Rift and its adjacent terrane boundaries (Fig. 1B) represent major zones of pre-rift basement mechanical weakness that controlled the location, structure, and evolution of both the border and intra-basinal faults during the earliest phase of continental extension. We show how the geometry of the CSZ controlled along-rift variations in the early-phase tectonic extension and overall basin geometry, the effects of which persist through and thus influence the later rift geometry. We also expand our analysis to the nearby Luama Rift, which is coeval, colinear with, and parallel to the Rukwa Rift; both basins representing structural elements along a NW-trending Karoo-age rift branch herein referred to as “the Rukwa Trend" (Fig. 1A). Our results resolve a long-standing controversy related to the geometrical structure and kinematics of rifting in this part of the East African Rift System.

GEOLOGICAL SETTING

The Precambrian (Pre-Rift) Basement of the Rukwa Trend

The crystalline basement of the Rukwa Trend is composed of the metamorphic and igneous rocks of the Precambrian (1.95 -1.85 Ga) Ubendian Belt, which formed during the collision between the Archean Tanzania Craton and the Bangweulu Block, and which comprises the Ufipa, Katuma, Wakole, Lupa, Mbozi, Ubende, and Upangwa terranes (Figs. 1A-B; Lenoir et al., 1994). This orogenic belt is defined by several NW-trending granulite facies terranes (2.1-2.025 Ga) that are bounded by steeply dipping, ductile, amphibolite facies, strike-slip shear zones (Fig. 1B; Daly, 1988; Lenoir et al., 1994; Theunissen et al., 1996; Kolawole et al., 2018). The geochronology, geochemistry, and metamorphic structure of the Ubendian Belt suggests it formed in response to multiple episodes of wrench tectonics and subduction events extending from the Paleoproterozoic to the Neoproterozoic (Theunissen et al., 1996; Ganbat et al., 2021). Neoproterozoic eclogites within the orogenic belt revealed the existence and location of the Chisi Suture Zone (CSZ), which has been identified as the primary Neoproterozoic subduction suture between the Tanzania and Bangweulu cratons (Fig. 2A; Lenoir et al., 1994; Boniface & Schenk, 2012).

The NW-trending metamorphic fabrics in the bounding terranes are exposed in basement exposures along the flanks of Rukwa Rift and they are suggested to have exerted some control on the development of the basin (Wheeler and Karson, 1994; Theunissen et al., 1996; Boven et al., 1999; Lemna et al., 2018; Heilman et al., 2019). The magnetic-high anomaly expression of the CSZ indicates the presence of highly magnetized eclogitic crust, and the associated lineament extends southeast beneath the Rukwa Rift, sub-parallel to the northwest trend of the rift (Figs. 1B; Heilman et al., 2019; Lemna et al., 2019).

Phanerozoic Rifting along the Rukwa Trend

The present-day configuration of the Rukwa Trend consists of multiple colinear, NNW-trending rift basins (Rukwa, Karonga, and Luama basins) that initially developed during Permo-Triassic (Karoo) phase of rifting (e.g., Delvaux, 2001). All three basins were reactivated by extensional tectonics in the Cretaceous (Roberts et al., 2010, 2012). However, only the Rukwa Rift and Karonga Basin (Fig. 1A) experienced significant reactivation in the Cenozoic, and they are still currently active (e.g., Morley et al., 1999; Delvaux, 2001; Chorowicz, 2005). The Rukwa Rift, the primary focus of this study, currently defines a graben and is bounded to the northeast by the Lupa Fault and to the southwest by the Ufipa Fault (Fig. 2B). However, the basin initially developed as a NE-dipping half graben (with a shallow graben geometry only in the NW) during the Karoo rifting phase, bounded to the northeast by the principal border fault, the Lupa Fault (Figs. 2C-D). The Karoo intra-basinal faults (KIF) and basement highs predominantly trend NNW, oblique to the Lupa Fault strike (Fig. 2B). Estimates of the Karoo-age extension direction vary from NE-SW to E-W (Fig. 2B).

DATASET AND METHODOLOGY

Along the Rukwa Trend, we compile structural mapping and measurements from published 2-D seismic data (e.g., Fig. 2C) and integrate these with aeromagnetic data (Figs. S1A-B) and satellite radar digital elevation model (DEM) (Figs. S2A-B). We use aeromagnetic data to map key pre-rift intra-basement structures along the axis of the Rukwa Rift and along-trend of the rift. We applied mathematical filters and transforms to the aeromagnetic grid to enhance structural features and to estimate the depths to magnetic sources in the basement (see supplementary information).

We establish the initial (i.e., Karoo rift phase) geometry of the Rukwa Rift and related faults using published seismic reflection profiles, and associated fault trace maps and sediment thickness maps ('Karoo Isopach') presented by Morley et al. (1992, 1999). We also calculate along-rift variations in Karoo-age tectonic extension (backstripped to Karoo time surface; Fig. 4C) accommodated by slip on the Lupa Fault and intra-basinal faults, again using data published by Morley et al. (1992). We integrate these structural data with aeromagnetic data analysis to investigate the influence of the pre-rift basement structure on the early phase structure and evolution of the Rukwa Rift.

RESULTS

3-D Geometry and Extent of the CSZ

The petrology, local structure, and topographic expression of the CSZ is well-constrained in the Chisi area, located on the NW flank of the Rukwa Rift (Figs. 1B and 2A; Theunissen et al., 1996 and Boven et al., 1999; Boniface & Schenk, 2012). Field observations show that the CSZ is dominated by steep, NE- and SW-dipping, metamorphic fabrics (Fig. 2A). At this location, the CSZ is characterized by a prominent NW-trending, positive magnetic anomaly lineament (Fig. 1B) and a topographic ridge (Figs. S2A and 2A). Based on its distinct geophysical and geomorphic expression, we map the northwestward and southeastward continuations of the CSZ beneath the Rukwa Rift and the NW boundary zone of the Luama Rift (Fig. 1B).

Northwest of the Chisi area, the CSZ associated structures (i.e., the magnetic-high anomaly lineament and topographic ridge) appear to split into two branches, the East and West CSZ Splays (Fig. 1B). The West CSZ Splay is colinear with the subaerial Mahale Ridge and the Kavala Island Ridge, which is presently buried beneath Lake Tanganyika and that continues northwest into the Busindi Ridge, which itself represents the footwall of the Busindi border fault of the Luama Rift (Fig. 1B, S2A). The West CSZ Splay is delineated by a magnetic-high anomaly lineament that rotates NNW and continues north to apparently link with the Ubwari Ridge (buried horst and subaerial peninsula; Figs. 1B, S1A-B). Although the Ubwari Ridge is a fault-bounded horst block in the Cenozoic Tanganyika Rift, its spatial and perhaps genetic association with the CSZ is based on both the colinearity with the continuation of the magnetic-high anomaly lineament of the CSZ, and the southeastward rotation of the N-trending metamorphic fabrics of the subaerial section of the horst (Figs. S1B and S2B).

The CSZ extends southeastwards from the Chisi area to continue beneath the Rukwa Rift, where it is sub-parallel to the rift border faults (Figs. 1B and 2A). Just southeast of the termination of the CSZ magnetic lineament, the Mughese Shear Zone which separates the Ufipa and Mbozi Terranes of the Ubendian Belt (Fig. 1B), extends beneath the Musangano Trough (bifurcation of the Rukwa Rift) and continues southeast into the Karonga Basin (Figs. 1B, 2B). Overall, the CSZ-associated aeromagnetic and geomorphic structures extend for >600 km from the Luama and Tanganyika rifts, southeastwards through the Rukwa Rift (Fig. 1B). Although our mapping suggests an along-trend and perhaps genetic relationship between the CSZ and the Mughese Shear Zone (Fig. 1B), we clarify that at the time of this contribution, there is no available data confirming that the Mughese Shear Zone is also a subduction-related suture. In the absence of this information, we define the southeast termination of the CSZ as the termination zone of its magnetic anomaly lineament beneath the Rukwa Rift (Figs. 1B and 3A).

Our 3D grid of the depth-distribution of intra-basement magnetic sources along the Rukwa Rift (Figs. 3A-C, S3A-B, S4A-B) reveal a steeply-dipping, NW-trending zone of magnetic sources that extend to 12 km depth; this feature is spatially collocated with the surface trend of the CSZ aeromagnetic lineament (Fig. 3B). Northeast of these CSZ-related magnetic sources, a narrow sub-vertical block of very shallow (<6 km deep) magnetic sources is spatially colocated with the Lupa Fault. This zone of Lupa Fault-related shallow sources separates the CSZ-related sources from another sub-vertical cluster of moderately deeper (~9 km-deep) magnetic sources that are spatially colocated with the Katuma Terrane (Figs. 3B-D).

The CSZ and the Early-rift (Karoo) Structure

The Karoo-age basin of the Rukwa Rift widens southeastwards from c. 16 km to c. 57 km at the terminus of the CSZ magnetic lineament, before narrowing to <16 km towards the southeast (Fig. 2B). The Karoo intra-basinal faults (KIF, 329°±9.6) are dominated by a fault cluster, spaced 4-6 km apart and striking oblique to the Lupa Fault (311°). The fault cluster is collocated with the CSZ magnetic lineament and trends parallel to the lineament (Figs. 2C; 4A-B). Although, some of the KIF faults dip to the SW, most of them dip to the NE (Fig. 2B). A Karoo isopach map shows that the thickest sections (>1 km-thick) of the Karoo-age units are generally confined to the northeast of the CSZ anomaly (yellow polygon in Fig. 2B; also see Figs. 2C-D). Adjacent to CSZ magnetic lineament beneath the Rukwa Rift (i.e., northwestern section of the rift), the Lupa Fault has a relatively high dip (~69°); this decreases south-eastwards to ~46° (Fig. 4C). Also, within the rift, prominent basement ridges cluster along the CSZ, some of which appear to be fault-bounded (Fig. 2B).

Strain Distribution within the Rukwa Rift during Karoo Extension

The proportion of Karoo-phase tectonic extension accommodated by the KIF increased southeastwards during the earliest stages of rifting in the Rukwa Rift (Figs. 4C-D). This trend was coincident with an increase in across-strike separation between the Lupa border fault and the CSZ, from <10 km in the NW to ~30 km at the terminus of CSZ anomaly (Fig. 4C; see also Fig. 4A). However, from the southeast of the termination of the CSZ to the southeast tip of the basin, total extension was largely accommodated by the Lupa Fault (Fig. 4C). This anomalous localization of relatively greater Lupa Fault extension to the southeast was consistent with the significant increase in throw gradient on the fault, given by an increase from ~0.04 northwest of the CSZ magnetic anomaly terminus, to ~0.16 southeast of the terminus (Fig. 4C).

CONTROLS OF THE CSZ AND TERRANE BOUNDARY ON EARLY-RIFT FAULTING, STRAIN DISTRIBUTION, AND BASIN ARCHITECTURE

Border Fault Development

The geometrical and spatial relationships between the Karoo rift-related structures, the CSZ, and the adjacent basement terrane boundaries reveal how strain was localized and spatially partitioned during the early phases of extension in the Rukwa Rift. The Lupa Fault is the largest rift-related structure in the Rukwa Rift, having formed at the very onset of rifting, thus representing the border fault (e.g., Morley et al., 1992, 1999; Kilembe and Rosendahl, 1992; Wheeler and Karson 1994). Studies suggest that the Lupa Fault localized along terrane boundaries (Katuma-Wakole boundary in the NW and Lupa-Mbozi boundary in the SE) and that its northeastern geometry is influenced by the structural fabrics in the bounding Katuma Terrane (Figs. 1B, 3B-D; Daly, 1988; Wheeler and Karson, 1994; Theunissen et al., 1996; Lemna et al., 2018; Heilman et al., 2019). However, the observations supporting these hypotheses were based on the shallow geometries of structures observed in the field or the plan-view structural trends of metamorphic fabrics expressed in aeromagnetic data. However, the sub-vertical dips described by the deeper cluster of magnetic sources beneath the Katuma Terrane (Fig. 3B) and observations of steep dips along the other terrane boundaries within the mobile belt (e.g., Theunissen et al., 1996; Kolawole et al., 2018) suggest that the Katuma-Wakole terrane boundary is most likely a steeply dipping structure. Therefore, based on the prominence of significantly steeper dips along the northwestern sections of the Lupa Fault adjacent to the Katuma Terrane, and less steep dips in the SE, past the Katuma Terrane termination (Figs. 3B-C, 4C, 5A), we suggest that both the large-scale 3-D geometry of the Katuma-Wakole Terrane boundary and the tectonic structures in the Katuma Terrane strongly influenced the 3-D geometry of the Lupa border fault along its NW section.

The sub-vertical dip of the CSZ-related magnetic sources and southwest dip direction of the Lupa Fault (Fig. 3C) also suggests that the deepest sections of the border fault could merge with the suture zone at the deeper crustal levels, although it would require a southwestward dip for the CSZ at depth. If this spatial and potentially kinematic relationship is true, we infer a depth-dependent partitioning of the control of structural inheritance on the early development of the Lupa border fault, such that the upper sections of the fault exploited the Katuma-Wakole Terrane boundary and structures in the Katuma Terrane, and the deepest section exploited the Chisi Suture Zone.

Intra-Basinal Faulting

The collocation and parallel trends of the KIF and CSZ suggest that the CSZ largely controlled the localization of the Karoo intra-basinal faulting (Fig. 4A and 5A). The prominence of NE-dip direction of the KIF faults (Fig. 4A) suggests that the KIF exploited the NE-dipping metamorphic fabrics along the CSZ (Fig. 2A). The confinement of the main Karoo-age rift fill between the Lupa Fault and CSZ (where present) (Fig. 5A) indicates that the KIF cluster directly influenced the first-order sediment distribution during the early phases of extension. The Karoo-age basin is widest in the northwest where the CSZ is present (CSZ rotates from NW to NNW trend, away from the Lupa Fault), further indicating the influence of the CSZ and its geometry on the extent of the early rift-related depocenter (Fig. 4A). The apparent confinement of earliest rift-related sediments also provides further age constraints on the timing of formation of the intra-basinal fault cluster. Overall, these observations indicate that the suture zone and terrane boundary represent discrete zones of inherited mechanical weakness in the crust where brittle deformation was accommodated during the early stages of continental extension.

Early-Rift Paleotopography

The Karoo-age rift topography is likely dominated by the footwall uplift along the Lupa border fault in the northeastern basin margin. However, the clustering of basement ridges along the submarine part of the CSZ, likely representative of early syn-rift erosionally-resistant topography, is consistent with observations of topographic ridges along the CSZ onshore (Figs. 1B and S2A). Elsewhere, prominent, erosionally-resistant topographic ridges define the surface expression of the Mughese Shear Zone (Kolawole et al., 2018), which appears to be a southeast continuation of the CSZ trend in the Karonga Basin (Fig. 1B). Such ridges represent elevated topographic domains that may represent important sediment sources (e.g., Gawthorpe and Leeder, 2000). Thus, the chain of ridges along the CSZ represent intra-basinal sediment-source regions near the southwestern basin margin, indicating an additional importance of the CSZ during initial sedimentation in the Rukwa Rift.

Early-Rift Distribution of Extension

Our analyses show that within the northwestern section of the basin, Karoo-age tectonic extension was largely accommodated on both the CSZ-related intra-basinal faults (KIF) and the Lupa border fault (Figs. 4C-D); in fact, during this initial phase of extension, more strain was accommodated on intra-basinal faults than the (developing) border fault. In contrast, southeast of the CSZ termination beneath the basin (or at significantly large separation distance), extension was primarily accommodated along the Lupa border fault. These suggest that during the early phase of rifting, there was a competition for extensional strain localization between the CSZ and the Katuma-Wakole terrane boundary in the northwest. Due to the southward increase in separation between the CSZ and Katuma-Wakole/Lupa-Mbozi terrane boundaries, and the absence of CSZ in the southeastern section of the Karoo-age basin, tectonic extension was then primarily accommodated along the Lupa Fault, which ultimately exploited the Lupa-Mbozi terrane boundary (Fig. 4C-D). The significant increase in the Lupa Fault Top-basement offset just south of the CSZ termination (Fig. 4C) also supports the dominant localization of extensional strain on the border fault in the southeastern section of the basin where the CSZ-related KIF is absent. Thus, we suggest that the CSZ strongly controlled the early-phase distribution of tectonic extension along the Rukwa Rift.

This along-rift partitioning of strain resulted in a lateral change of the overall Karoo-age rift geometry from a shallower graben in the northwest, to a deep half graben in the southeast. Although this along-rift change in rift geometry was previously thought to be primarily related to variation in border fault strain accommodation controlled by oblique extensional kinematics (Morley et al., 1992), we here suggest that it is primarily controlled by the focusing of extensional strain along prominent pre-existing discrete zones of basement weakness during the early phase of rifting. This resolves a long-standing controversy related to the geometrical structure and kinematics of rift faulting in the Rukwa Rift. Elsewhere along the Rukwa Trend, farther northwest of the Rukwa Rift, the Busindi border fault of the Luama Rift exploited the NW continuation of the CSZ (Figs. 1B and 3D), demonstrating the broader influence of the CSZ on the development of the other Karoo rift segments of the Rukwa Trend. In the Tanganyika Rift, the along-rift distribution of tectonic extension is influenced by the lateral variation of the inherited crustal rheology (Wright et al., 2020), further demonstrating the strong influence of structural inheritance on the early localization and distribution of extension along continental rifts.

Post-Karoo Rift Architecture

The CSZ and adjacent terrane boundaries continued and still continue to influence rift geometry long after the Karoo phase of extension. First, the mean trend of all the intra-basinal faults generally remains the same during the Cenozoic phase of rifting (Figs. 4B and 5B; Morley et al., 1992; Kilembe and Rosendahl, 1992). Second, the along-strike projection of the CSZ southeast of its magnetic anomaly termination is coincident with location and orientation of the Musangano Trough, which represents a southeastward continuation of the Rukwa Rift during the Cenozoic rifting phase (Fig. 5A). We suggest that the extension of the KIF to the CSZ termination zone already established the incipient graben of the Musangano Trough during the Karoo rifting phase (Figs. 5A and 6). We suggest that the CSZ and its colinear Mughese Shear Zone, along which the Musangano Trough developed (Fig. 5A), both constitute coupled discrete zones of weakness in the basement that accommodated the continuous lateral southeastward propagation of the KIF as a narrow graben during the post-Karoo phases of extension. Thus, the present-day bifurcation of the Rukwa Rift into the Songwe and Musangano troughs (Fig. 1C) was established during the very earliest stage of rifting. In addition, the southeastern border fault of the Rukwa Rift (Ufipa Fault; Fig. 2B) which developed in the Cenozoic, largely exploited the tectonic fabrics of the Ufipa Terrane (Heilman et al., 2019).

More broadly, in the Cenozoic Tanganyika Rift, located northwest of the Rukwa Rift (Figs. 1A-B), the rift basin is segmented (Sander and Rosendahl, 1989; Muirhead et al., 2019; Wright et al., 2020), with the segmentation occurring at the two northwestern CSZ splays (Fig. 1B). The Ruzizi and East Kigoma sub-basins are separated by the northern section of the East CSZ splay, whereas the East and West Kigoma sub-basins are separated by the southern section of the East Splay, and the West Kigoma and Kalemie Sub-basins are separated by the West CSZ splay. In essence, the

CSZ not only influenced the early-phase architecture of the Karoo-age Rukwa and Luama rift basins, but also the structure of the younger Tanganyika Rift. The spatial collocation of Cenozoic hydrothermal vents within different sections of the CSZ in the Tanganyika Rift (diamond symbols in Fig. 1B) highlights the deep reaches of the rift faults that exploited the basement weakness of the suture zone.

IMPLICATIONS FOR EARLY-STAGE ARCHITECTURE OF CONTINENTAL RIFT SYSTEMS

Our study of the Rukwa Rift suggest that early-phase rift strain is not accommodated by distributed normal faulting as suggested by classic models for continental extension (e.g., Gawthorpe and Leeder, 2000; Naliboff et al., 2017), but it is localized onto pre-existing structures via two different styles with associated deformational mechanisms. One style (Style-1 strain localization) is the localization of a large rift fault onto a narrow discrete zone of basement weakness, such as prominent basement terrane boundaries (this study), pre-existing fault zones, and narrow ductile shear zones, in which case the structures of the weak zone and the fabrics of the adjacent basement may influence the fault geometry (Fig. 6). An example of this is the development of the Livingstone Fault in Northern Malawi Rift (Wheeler and Karson, 1989), the Thyolo border fault in the Shire Rift Zone (Wedmore et al., 2020b), and splay faulting at a terrane boundary during the Late Cretaceous extension between Zealnadia and Australia (Phillips and McCaffrey, 2019b). A second style (Style-2 strain localization) is the localization of a fault cluster (linear, splay, or diffused fault strands) onto a broader discrete zone of basement weakness, such as pre-rift subduction suture zones (this study) or large batholiths, in which case the individual fault strands may exploit the smaller-scale mechanical heterogeneities within the broad zone of basement weakness (Fig. 6). An example of Style-2 localization is the development of tightly clustered faults that exploited the Precambrian Mughese Shear Zone along the western hinge margin (Karonga area) of the Northern Malawi Rift (Kolawole et al., 2018). Therefore, we hypothesize that during the earliest stages of continental rifting, strain initially localizes on pre-existing zones of crustal weakness, and the style of localization may be associated with the type of the inheritance and character of the inherited structure. In addition, we note that whilst pre-existing structure may exert a strong control on strain distribution and localization during the earliest phase of continental extension, the established early rift template, may persist through the subsequent phases of the stretching stage of rifting (i.e., prior to the necking and hyper-extension stages).

CONCLUSIONS

We investigated the distribution of strain during the earliest phase of extension in the Rukwa Rift, a Phanerozoic multiphase magma-poor rift basin that developed along the trend of the Precambrian Chisi Suture Zone (CSZ) and terrane boundary shear zones in East Africa.

Here are our main findings:

1) During the earliest phase of extension, although the border fault, Lupa Fault exploited the colinear Katuma-Wakole and Lupa-Mbozi terrane boundaries, the CSZ facilitated the early localization and development of a prominent intra-basinal fault cluster.

2) In the northwestern section of the rift, the presence and proximity of the CSZ and the Katuma-Wakole terrane boundary facilitated a competition for strain localization between the CSZ and the adjacent terrane boundary, whereas in the southeastern section where the CSZ is either absent or at a significantly large distance, strain is primarily localized along the Lupa-Mbozi terrane boundary.

3) The along-rift variation in early phase rift geometry, rift margin paleotopography, and depocenter extents were largely controlled by the CSZ.

4) The along-rift distribution of early-phase extension was largely influenced by structural inheritance, such that in the northwestern section of the rift, significant extension is accommodated by the intra-basinal fault cluster that exploited the CSZ, whereas in the southeast, extension is largely accommodated by the Lupa border fault.

5) Two styles of early-phase strain localization in which a.) strain is localized onto a narrow discrete zone of basement weakness in the form of a large rift fault (Style-1 strain localization), and b.) strain is localized onto a broad discrete zone of basement weakness in the form of a fault cluster (Style-2 strain localization).

6) Whilst pre-existing basement structure may exert the strong control on strain distribution and localization during the earliest phase of extension, the established early rift template, may persist through the subsequent phases of the stretching stage of rifting.

Our findings offer a window into the early stages of continental extension along a young evolving rift, revealing the influence of structural inheritance on early phase rift geometry and along-rift partitioning of strain along magma-poor rift basins.

ACKNOWLEDGMENTS

We thank the South Africa Development Council (SADC) for providing the aeromagnetic data to EA used in this study. The SADC aeromagnetic data is archived at http://sadc-gla.org/SADC/home.html. We have provided uninterpreted versions of the aeromagnetic data in our supplementary document. The seismic reflection cross-section of the Rukwa Rift shown in

this study (Fig. 2C) and other 2-D seismic datasets from the basin are archived in the appendix of Morley et al. (1999).

REFERENCES CITED

Agostini, A., Bonini, M., Corti, G., Sani, F. and Mazzarini, F., 2011. Fault architecture in the Main Ethiopian Rift and comparison with experimental models: implications for rift evolution and Nubia–Somalia kinematics. Earth and Planetary Science Letters, 301(3-4), pp.479-492.

Buiter, S.J.H., Torsvik, T.H., 2014. A review ofWilson Cycle plate margins: a role for mantle plumes in continental break-up along sutures? Gondwana Research 26, 627–653.

Chorowicz, J., 2005. The east African rift system. Journal of African Earth Sciences, 43(1-3), 379-410.

Christian Schiffer, Anthony G. Doré, Gillian R. Foulger, Dieter Franke, Laurent Geoffroy, Laurent Gernigon, Bob Holdsworth, Nick Kusznir, Erik Lundin, Ken McCaffrey, Alexander L. Peace, Kenni D. Petersen, Thomas B. Phillips, Randell Stephenson, Martyn S. Stoker, J. Kim Welford (2019) Structural inheritance in the North Atlantic. Earth-Science Reviews.

Claringbould, J. S., Bell, R., Jackson, C. A., Gawthorpe, R., & Odinsen, T. (2019). Complex strain partitioning and heterogeneous extension rates during early rifting in the East Shetland Basin, northern North Sea. EarthArxiv. https://doi.org/10.31223/osf.io/nbe2c

Daly, M. C. (1988). Crustal shear zones in central Africa—A kinematic approach to Proterozoic tectonics. Episodes, 11(1), 5–11.

Daly, M. C., Chorowicz, J., & Fairhead, J. D. (1989). Rift basin evolution in Africa: The influence of reactivated steep basement shear zones. Geological Society, London, Special Publications, 44(1), 309–334.

Delvaux, D., 2001. Karoo rifting in western Tanzania: Precursor of Gondwana breakup. Contributions to geology and paleontology of Gondwana in honor of Helmut Wopfner: Cologne, Geological Institute, University of Cologne, 111-125.

Delvaux, D., Kervyn, F., Macheyeki, A. S., & Temu, E. B. (2012). Geodynamic significance of the TRM segment in the East African Rift (W-Tanzania): Active tectonics and paleostress in the Ufipa plateau and Rukwa basin. Journal of Structural Geology, 37, 161–180.

Dewey, J., Spall, H., 1975. Pre-Mesozoic plate tectonics: how far back in Earth history can the Wilson Cycle be extended? Geology 3, 422–424.

Ganbat, A., Tsujimori, T., Boniface, N., Pastor-Galán, D., Aoki, S. and Aoki, K., 2021. Crustal evolution of the Paleoproterozoic Ubendian Belt (SW Tanzania) western margin: A Central African Shield amalgamation tale. Gondwana Research, 91, pp.286-306.

Gawthorpe, R.L. and Leeder, M.R., 2008. Tectono-sedimentary evolution of active extensional basins. Basin Research, 12(3-4), pp.195-218.

Heilman, E., Kolawole, F., Atekwana, E. A. and Mayle, M., 2019. Controls of Basement Fabric on the Linkage of Rift Segments. Tectonics, 38(4), pp.1337-1366.

Hodgson, I., Illsley-Kemp, F., Gallacher, R.J., Keir, D., Ebinger, C.J. and Mtelela, K., 2017. Crustal structure at a young continental rift: A receiver function study from the Tanganyika Rift. Tectonics, 36(12), pp.2806-2822.

Kilembe, E.A. and Rosendahl, B.R., 1992. Structure and stratigraphy of the Rukwa rift. In: C.J. Ebinger, H.K. Gupta and 1.0. Nyambok (Editors), Seismology and Related Sciences in Africa. Tectonophysics, 209: 143-158.s

Kolawole, F., Atekwana, E.A., Laó-Dávila, D.A., Abdelsalam, M.G., Chindandali, P.R., Salima, J. and Kalindekafe, L., 2018. Active deformation of Malawi rift's north basin Hinge zone modulated by reactivation of preexisting Precambrian Shear zone fabric. Tectonics, 37(3), 683-704.

Lee, H., Fischer, T.P., Muirhead, J.D., Ebinger, C.J., Kattenhorn, S.A., Sharp, Z.D., Kianji, G., Takahataf, N., Sano, Y., 2017. Incipient rifting accompanied by the release of subcontinental lithospheric mantle volatiles in the Magadi and Natron basin, East Africa. J. Volcanol. Geotherm. Res.346, 118–133.

Lemna, O.S., Stephenson, R. and Cornwell, D.G., 2019. The role of pre-existing Precambrian structures in the development of Rukwa Rift Basin, southwest Tanzania. Journal of African Earth Sciences, 150, 607-625.

Lenoir, J.L., Liégeois, J.P., Theunissen, K. and Klerkx, J., 1994. The Palaeoproterozoic Ubendian shear belt in Tanzania: geochronology and structure. Journal of African Earth Sciences, 19(3), pp.169-184.

Muirhead, J.D., Kattenhorn, S.A., Lee, H., Mana, S., Turrin, B.D., Fischer, T.P., Kianji, G., Dindi, E., Stamps, D.S., 2016. Evolution of upper crustal faulting assisted by magmatic volatile release during early-stage continental rift development in the East African Rift. Geosphere, 12, 1670–1700.

Muirhead, J.D., Wright, L.J. and Scholz, C.A., 2019. Rift evolution in regions of low magma input in East Africa. Earth and Planetary Science Letters, 506, pp.332-346.

Morley, C.K., 2010. Stress re-orientation along zones of weak fabrics in rifts: An explanation for pure extension in 'oblique' rift segments?. Earth and Planetary Science Letters, 297(3-4), pp.667-673.

Morley, C.K., Cunningham, S.M., Harper, R.M. and Wescott, W.A., 1992. Geology and geophysics of the Rukwa rift, East Africa. Tectonics, 11(1), pp.69-81.

Morley, C.K., Wescott, W.A., Harper, R.M. and Cunningham, S.M., 1999. Geology and geophysics of the Rukwa Rift. Geoscience of Rift Systems-Evolution of East Africa. AAPG Studies in Geology, 44, pp.91-110.

Naliboff, J.B., Buiter, S.J., Péron-Pinvidic, G., Osmundsen, P.T. and Tetreault, J., 2017. Complex fault interaction controls continental rifting. Nature communications, 8(1), pp.1-9.

Osagiede, E.E., Rotevatn, A., Gawthorpe, R., Kristensen, T.B., Jackson, C.A. and Marsh, N., 2020. Pre-existing intra-basement shear zones influence growth and geometry of non-colinear normal faults, western Utsira High–Heimdal Terrace, North Sea. Journal of Structural Geology, 130, p.103908.

Phillips, T.B., Fazlikhani, H., Gawthorpe, R.L., Fossen, H., Jackson, C.A.L., Bell, R.E., Faleide, J.I. and Rotevatn, A., 2019a. The Influence of Structural Inheritance and Multiphase Extension on Rift Development, the Northern North Sea. Tectonics, 38.

Phillips, T.B. and McCaffrey, K.J., 2019b. Terrane Boundary Reactivation, Barriers to Lateral Fault Propagation and Reactivated Fabrics: Rifting Across the Median Batholith Zone, Great South Basin, New Zealand. Tectonics, 38(11), 4027-4053.

Ragon, T., Nutz, A., Schuster, M., Ghienne, J.F., Ruffet, G. and Rubino, J.L., 2019. Evolution of the northern Turkana Depression (East African Rift System, Kenya) during the Cenozoic rifting: New insights from the Ekitale Basin (28-25.5 Ma). Geological Journal, 54(6), pp.3468-3488.

Roberts, E.M., O'Connor, P.M., Stevens, N.J., Gottfried, M.D., Jinnah, Z.A., Ngasala, S., Choh, A.M. and Armstrong, R.A., 2010. Sedimentology and depositional environments of the Red Sandstone Group, Rukwa Rift Basin, southwestern Tanzania: New insight into Cretaceous and Paleogene terrestrial ecosystems and tectonics in sub-equatorial Africa. Journal of African Earth Sciences, 57(3), pp.179-212.

Roberts, E.M., Stevens, N.J., O'Connor, P.M., Dirks, P.H.G.M., Gottfried, M.D., Clyde, W.C., Armstrong, R.A., Kemp, A.I.S. and Hemming, S., 2012. Initiation of the western branch of the East African Rift coeval with the eastern branch. Nature Geoscience, 5(4), pp.289-294.

Theunissen, K., Klerkx, J., Melnikov, A., & Mruma, A. (1996). Mechanisms of inheritance of rift faulting in the western branch of the East African Rift, Tanzania. Tectonics, 15(4), 776–790.

Versfelt, J.W. (2009), South Atlantic margin rift basin asymmetry and implications for pre-salt exploration. International Petroleum Technology Conference (IPTC) paper 13833, Doha, Qatar.

Wedmore, L.N., Biggs, J., Williams, J.N., Fagereng, Å., Dulanya, Z., Mphepo, F. and Mdala, H., 2020a. Active fault scarps in southern Malawi and their implications for the distribution of strain in incipient continental rifts. Tectonics, 39(3), p.e2019TC005834.

Wedmore, L.N., Williams, J.N., Biggs, J., Fagereng, Å., Mphepo, F., Dulanya, Z., Willoughby, J., Mdala, H. and Adams, B.A., 2020b. Structural inheritance and border fault reactivation during active early-stage rifting along the Thyolo fault, Malawi. Journal of Structural Geology, 139, 104097.

Wheeler, W.H. and Karson, J.A., 1989. Structure and kinematics of the Livingstone Mountains border fault zone, Nyasa (Malawi) Rift, southwestern Tanzania. Journal of African Earth Sciences (and the Middle East), 8(2-4), 393-413.

Wheeler, W.H. and Karson, J.A., 1994. Extension and subsidence adjacent to a" weak" continental transform: An example from the Rukwa rift, East Africa. Geology, 22(7), 625-628.

Wilson, J.T., 1966. Did the Atlantic close and then re-open? Nature 211, 676–681.

Wright, L. J. M., Muirhead, J. D., & Scholz, C. A. (2020). Spatiotemporal variations in upper crustal extension across the different basement terranes of the Lake Tanganyika Rift, East Africa. Tectonics, 39, e2019TC006019.

FIGURES

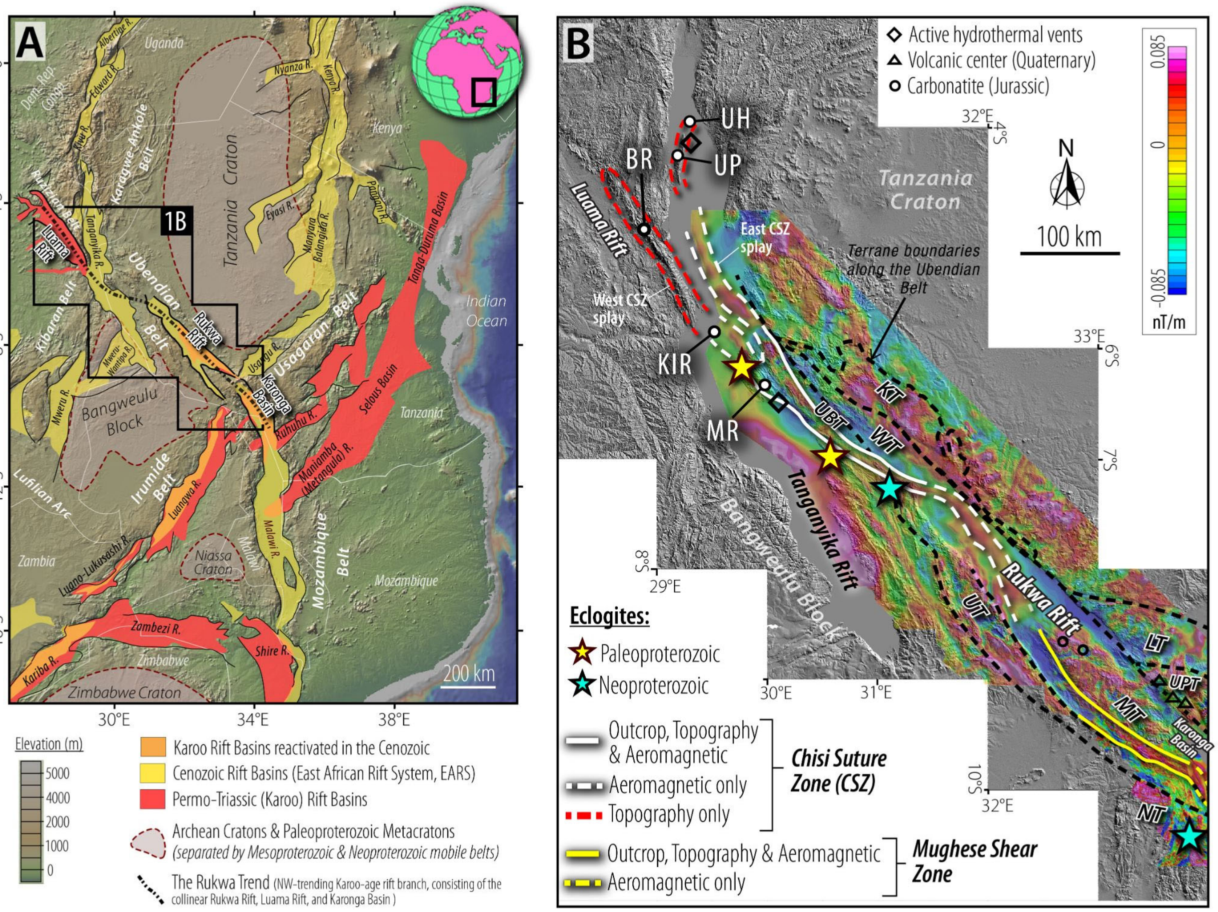

Figure 1. A: Map of east Africa showing the Permo-Triassic (i.e., Karoo rift system) rift segments, and the currently active rift segments (i.e., East African Rift System). **B:** Shuttle Radar Topography Mission (SRTM) Digital Elevation Model (DEM) hillshade covering the Rukwa Rift Trend, overlaid with the vertical derivative aeromagnetic of SW Tanzania. Black dashed lines represent boundaries of the Precambrian terranes of the Rukwa Rift Trend (after Daly, 1988; Delvaux et al., 2012; Lemna et al., 2018; Heilman et al., 2019). See uninterpreted aeromagnetic and hillshade maps in supplementary figures 1 and 2. Geomorphic features: BR (Busindi Ridge), KIR (Kavala Island Ridge), MR (Mahale Ridge), UP (Ubwari Peninsula), UH (Ubwari Horst). Terranes of the Ubendian Belt: KT (Katuma Terrane), LT (Lupa Terrane), MT (Mbozi Terrane), UBT (Ubende Terrane), UPT (Upangwa Terrane), UT (Ufipa Terrane), WT (Wakole Terrane). Locations of hydrothermal vents and Mesozoic-Cenozoic igneous centers (volcanics and carbonatites) are obtained from Hodgson et al. (2017).

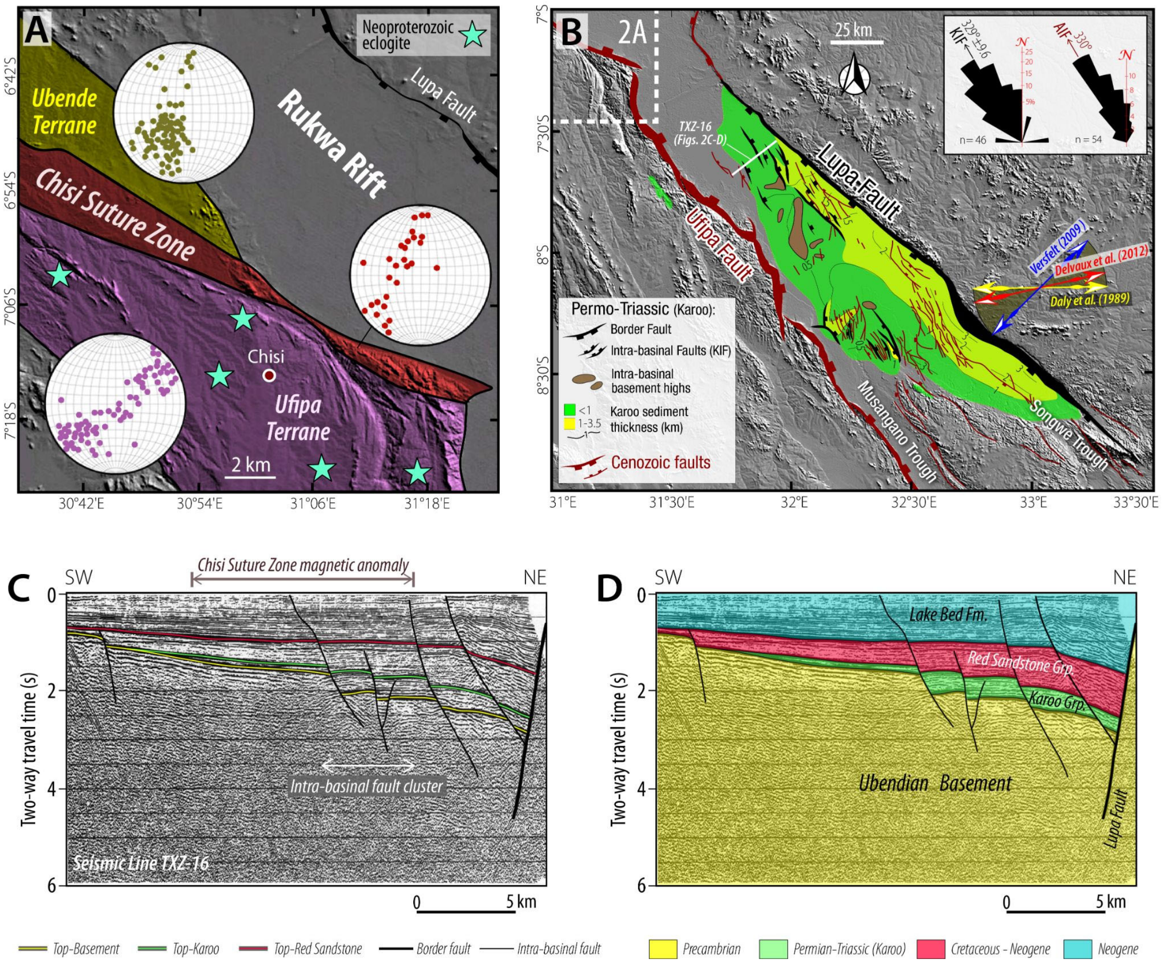

Figure 2. A: Satellite DEM hillshade of the NW Rukwa Rift shoulder (see Fig. 1A for location) showing the Precambrian Chisi Suture Zone outcrop, surrounding terranes and equal area stereographic projection (lower hemisphere) of the fold axes and planar structures representing the penetrative metamorphic fabrics as measured in field outcrops (after Theunissen et al., 1996; Boven et al., 1999; Boniface & Schenk, 2012). **B:** Map of the Rukwa Rift showing the interpreted Karoo and post-Karoo structural features. Structural features are from Morley et al., 1992, 1999). Arrows represent the previously published inferred Karoo extension directions. **C – D:** 2-D seismic line TXZ-16 and interpretation (modified from Morley et al., 1999) showing the major stratigraphic surfaces, the Lupa border fault, and intra-basinal faults.

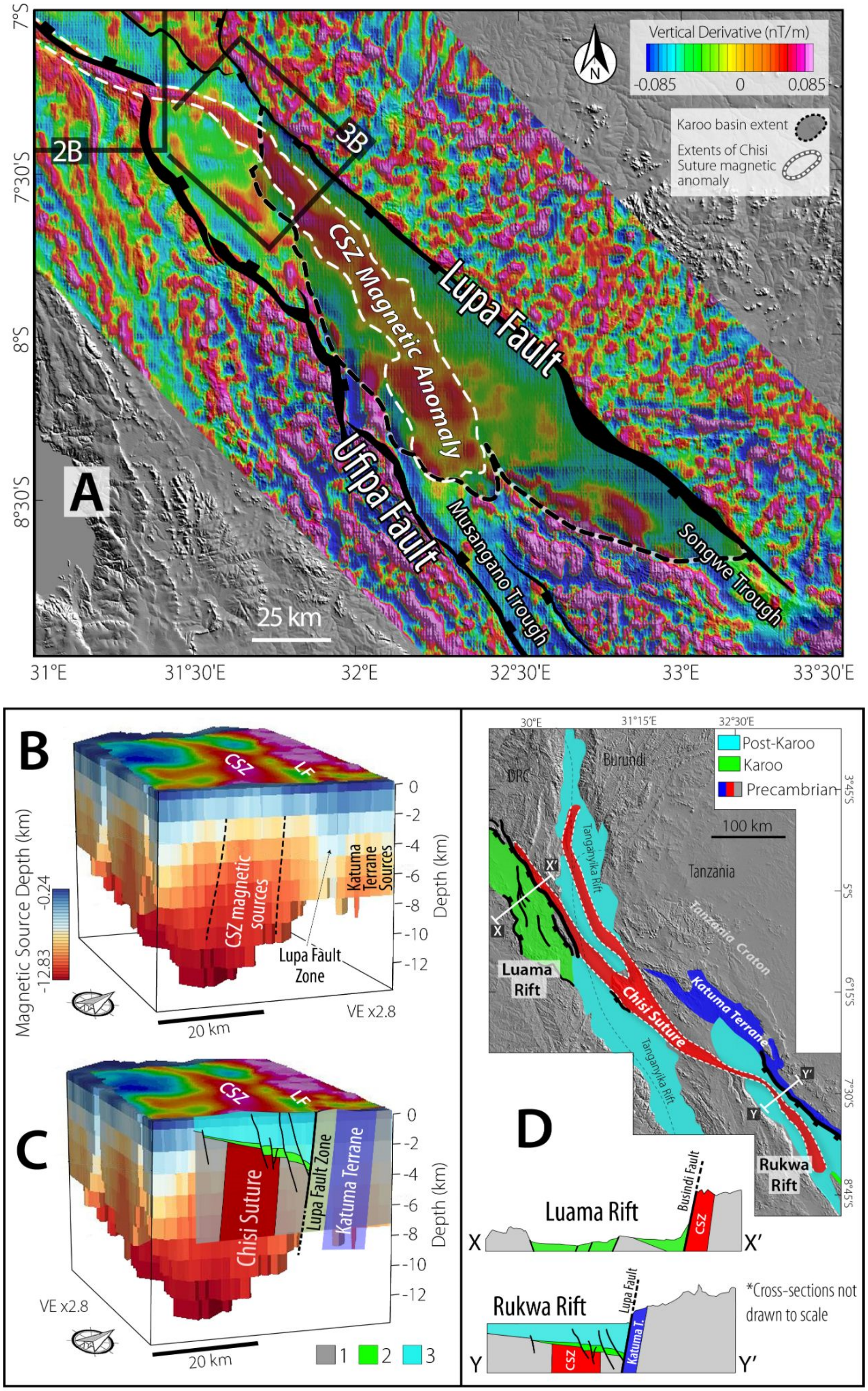

Vertical Derivative (nT/m)
-0.085
0
0.085
N
Karoo basin extent
Extents of Chisi Suture magnetic anomaly
2B
3B
CSZ Magnetic Anomaly
Lupa Fault
Ufipa Fault
Musangano Trough
Songwe Trough
A
25 km
7°S
7°30'S
8°S
8°30'S
31°E
31°30'E
32°E
32°30'E
33°E
33°30'E
B
CSZ
LF
Magnetic Source Depth (km)
-0.24
-12.83
CSZ magnetic sources
Lupa Fault Zone
Katuma Terrane Sources
Depth (km)
0
-2
-4
-6
-8
-10
-12
20 km
VE x2.8
C
Chisi Suture
Lupa Fault Zone
Katuma Terrane
1
2
3
30°E
31°15'E
32°30'E
Post-Karoo
Karoo
Precambrian
DRC
Burundi
Tanzania
Tanganyika Rift
Tanzania Craton
100 km
Luama Rift
Chisi Suture
Katuma Terrane
Rukwa Rift
3°45'S
5°S
6°15'S
7°30'S
8°45'S
X
X'
Y
Y'
D
Luama Rift
Businde Fault
CSZ
Rukwa Rift
Lupa Fault
Katuma T.
*Cross-sections not drawn to scale

Figure 3. A: Vertical derivative of the aeromagnetic grid overlaid on satellite Digital Elevation Model (DEM) hillshade, showing the rift border faults, rift shoulder basement fabrics and the aeromagnetic signature of the Chisi Suture Zone (CSZ) along the rift axis. See uninterpreted aeromagnetic maps in supplementary figure 1. **B:** 3-D gridded block of the Source Parameter Imaging (SPI) solutions from the transform of the aeromagnetic grid, showing the subsurface extents and geometry of CSZ and the shallower Katuma Terrane magnetic sources. **C:** 3-D gridded block overlaid with interpretations of the rift faults and simplified stratigraphy (interpretations from 2-D seismic line TXZ-16 of Morley et al., 1999 shown in Fig. 2C). Stratigraphic units shown: 1 (Precambrian basement), 2 (Karoo Grp. sequences), 3 (Post-Karoo sequences i.e., Red Bed Grp. and Lake Bed Fm.). **D:** Regional satellite DEM hillshade showing the >600 km extent of the CSZ and its relationship with the Rukwa and Luama segments of the Rukwa Trend. Cross-sections are based on satellite DEM (Luama Rift), and satellite DEM, aeromagnetics, and 2-D seismic data interpretation (Rukwa Rift).

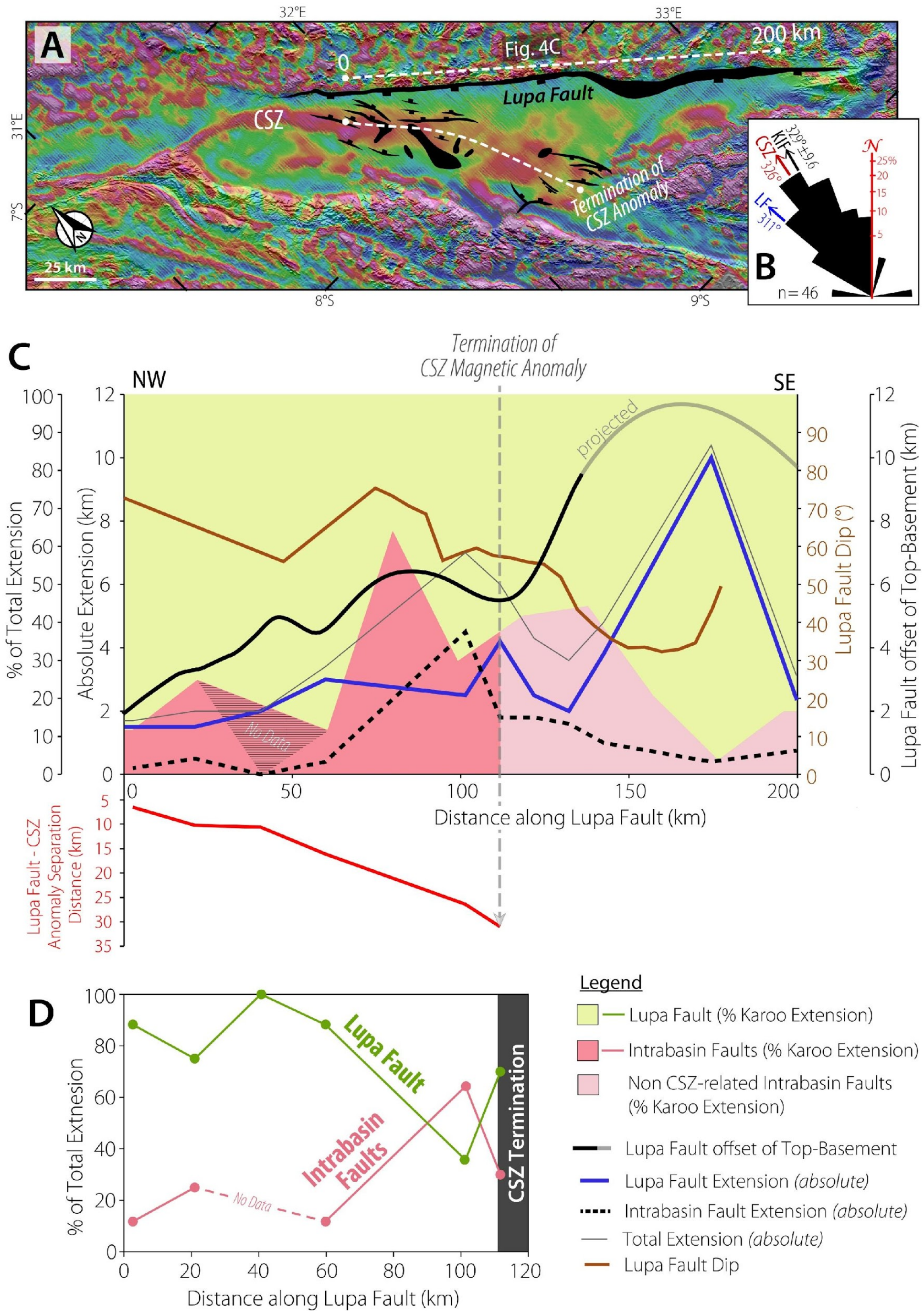

Figure 4. A: Map of vertical derivative of the aeromagnetic grid overlaid on satellite DEM hillshade, showing the segment of the Rukwa Rift on which Figures 3B-C are based. **B:** Frequency-azimuth distribution of the Karoo-age intra-basinal faults (KIF). CSZ = Chisi Suture Zone, LF = Lupa Fault **B:** Plot showing along-rift distribution of line-length measurement of the Top-Karoo surface as estimates of extension, Lupa Fault dip angle, and Top-Basement offset. **D:** Plot showing the along-rift variation of % of total extension accommodated by the Lupa Fault and the intra-basinal faults up till the CSZ termination (displayed as stacked area plot in 3C).

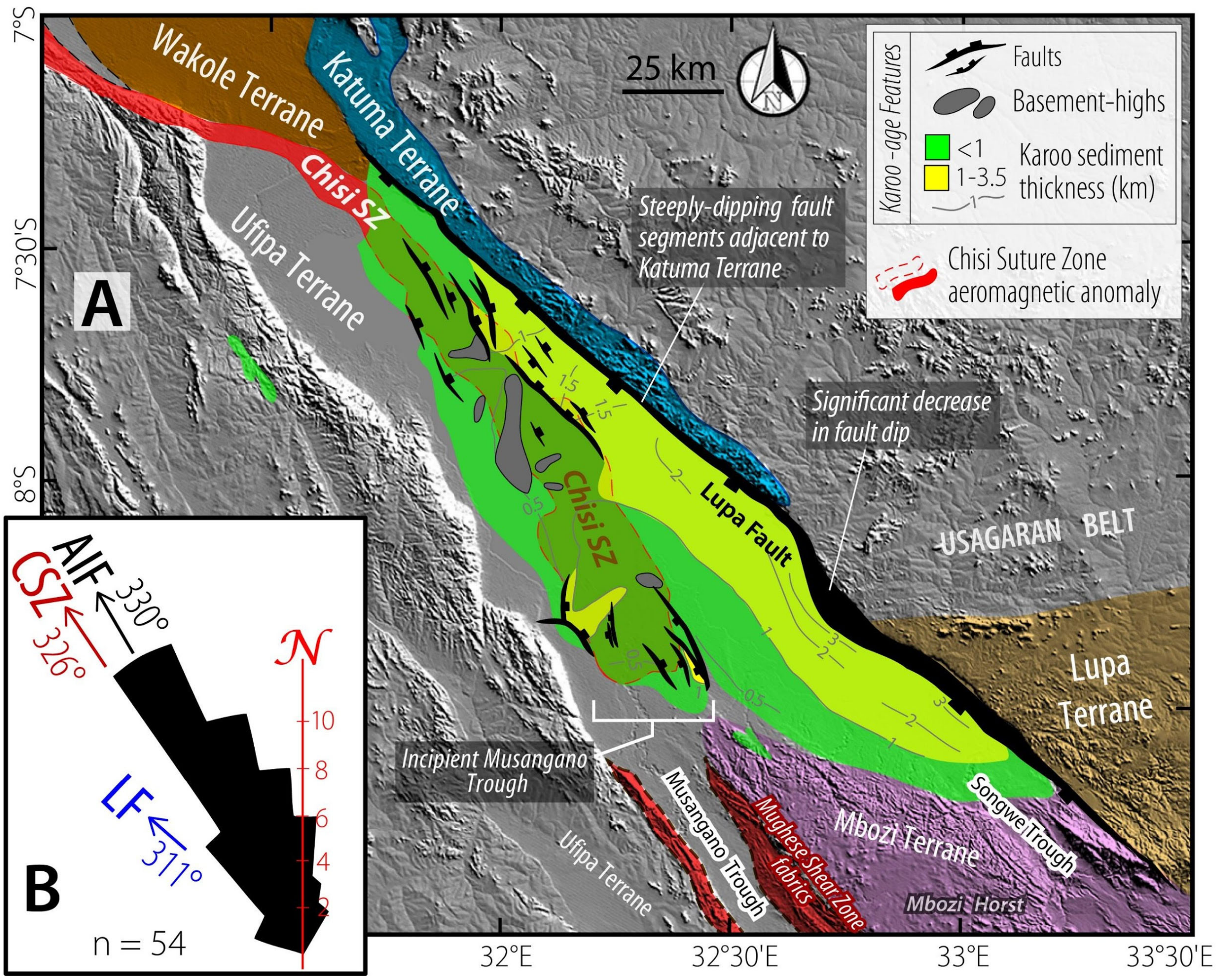

Figure 5. A: Satellite DEM hillshade of the Rukwa Rift, overlaid with the Karoo structural features (faults and basement ridges), Karoo isopach map (from Morley et al., 1992, 1999), Chisi Suture Zone magnetic anomaly, and the relevant surrounding basement terranes. **B:** Frequency-azimuth distribution of all the intra-basinal faults (Permian-Cenozoic) in the Rukwa Rift (after Morley et al., 1992). AIF = mean trend of all the intra-basinal faults, LF = approximate trend of the Lupa Fault, CSZ = approximate trend of the Chisi Suture Zone magnetic anomaly.

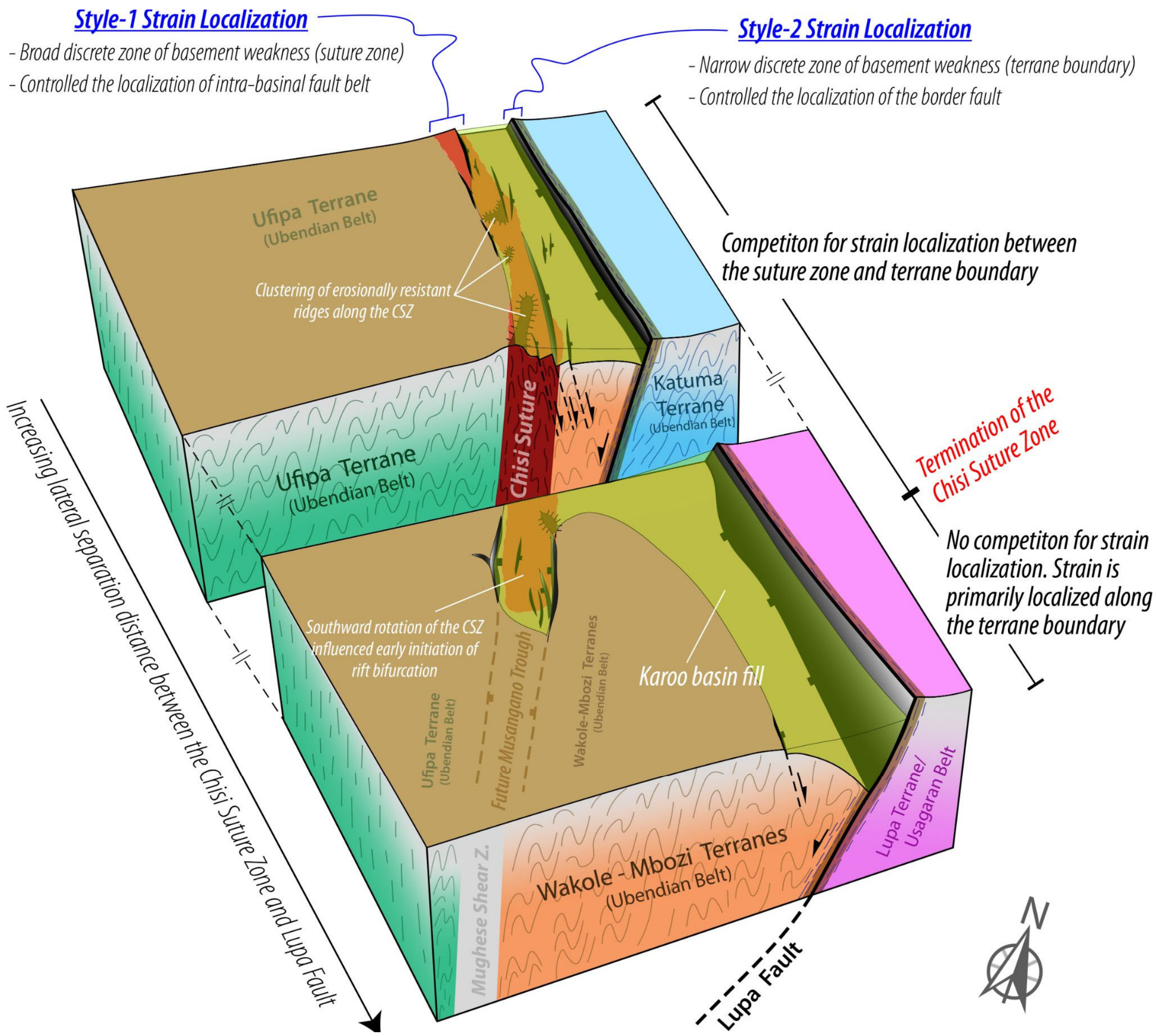

Figure 6. Cartoon illustrating some of the key observations in this study. The results of our study show how the structure of discrete zones of basement weakness influenced strain localization and along-rift distribution of extension during the early phases of rifting in the Rukwa Rift.

Supplementary Information

Contents of this document:

Supplementary Text 1.

Aeromagnetic Data, Satellite Topographic Data, and their Analyses:

The aeromagnetic data (Fig S1A), collected between 1977-1980 with flight height of 200 m and a flight line spacing of 1 km, was provided by the South Africa Development Council (SADC). First, we reduced the data to the magnetic pole (RTP) to correct for latitude-dependent skewness (Baranov, 1957), after which we applied a vertical derivative filter to better resolve magnetic gradients associated with structural features (Fig. S1B) (Salem et al., 2007; Kolawole et al., 2017, 2018; Heilman et al., 2019). In this study, we delineate the boundaries of the Chisi Suture Zone along the edges of the high magnetic anomaly lineament in the vertical derivative map of the aeromagnetic grid. In areas where aeromagnetic data is not available, we augmented the basement mapping with 30 m-resolution Satellite Radar Topographic Mission (SRTM) Digital Elevation Model (DEM) hill shade maps (Figs. S2A-B).

Depth to Magnetic Sources:

We assessed the subsurface continuity and dip geometry of prominent basement magnetic anomalies by calculating the depths to magnetic sources using two standard techniques which include the Source Parameter Imaging (SPI) and Euler Deconvolution techniques. The SPI transform of the aeromagnetic data (Thurston & Smith, 1997; Smith & Salem, 2005) assumes a step-type source model in which source depth is equal to an inverse of the peak value of the local wavenumber K over the step source. The SPI algorithm uses the horizontal (Dx and Dy) and vertical derivatives of the magnetic grid as input to compute the tilt derivative and K, from which it uses the peak values of K (using the Blakely test) to calculate the magnetic source depth solutions (e.g., Figs. S3A-B).

The Euler Deconvolution technique (Thompson, 1982; Reid et al., 1990; Stavrev and Reid, 2007) estimates the depth to a magnetic source by a derivation from Euler's homogeneity equation. The calculation relates the magnetic field of the source (given by the total magnetic intensity) and its gradient components (horizontal and vertical derivatives) to the location of the source of an anomaly. Also, the estimation is constrained by a structural index (SI) parameter which is a measure of the decay rate or homogeneity (for complex shapes) of the magnetic field with increasing distance from the source. The SI for magnetic fields varies from 0 to 3 depending on the assumed geometry of the source (i.e., contact/step, dipping sheet, cylinder, or sphere). For this study, we use SI = 1 (dipping sheet) and varied the maximum depth tolerance and window size for the calculations to produce minimum (Fig. S4A) and a maximum solution (Fig. S4B) for the magnetic source depths.

The 3-D tapering of the depth distribution of magnetic source depth solutions can delineate the 1^{st}-order geometry of dipping magnetic bodies (Mota et al., 2020). Therefore, for the purpose of integration with the aeromagnetic derivative map and seismic data interpretation, we present the results of the SPI calculations first as a 3-dimensional (3D) display of the source depth solutions (Figs. S1A-B) and a grid of the solutions, using the universal kriging algorithm (Olea, 1974). We present only the 3D grid of the SPI solutions (Figs. 3B-C of the main text) as it produced a better grid voxel due to the greater number of its solutions and tighter clustering of the deeper solutions, unlike the sparsely distributed solutions of the Euler Deconvolution results (Figs. S4A-B).

Results of the Magnetic Source Depth Calculations:

Overall, the results of the magnetic source depth calculations from both the SPI (Figs. S3A-B) and Euler Deconvolution (Figs. S3A-B) techniques show that the depth distribution of the magnetic sources in the basement describe a downward step-wise tapering towards the southwest. The magnetic sources below the Lupa Fault and its footwall (Katuma Terrane) are generally confined to shallower depths (< 7 km). Whereas, beneath the Chisi Suture Zone (CSZ) magnetic anomaly and to the SW of the anomaly, magnetic sources extend to deeper depths, up to 12 km. Thus, the 3D grid of the solutions (Figs. 3B-C) shows a steep tapering of the deeper magnetic sources beneath the CSZ. Overall, we emphasize that both techniques show a steep, southwestward increase in the depth extents of the basement magnetic sources. Thus, the southwestward tapering of the deeper solutions is interpreted to represent the southwest dip of the magnetic anomaly beneath the vicinity of the suture zone.

References:

Baranov, V. (1957). A new method for interpretation of aeromagnetic maps: Pseudo-gravimetric anomalies. Geophysics, 22(2), 359–382.

Kolawole, F., Atekwana, E.A., Malloy, S., Stamps, D.S., Grandin, R., Abdelsalam, M.G., Leseane, K. and Shemang, E.M., 2017. Aeromagnetic, gravity, and Differential Interferometric Synthetic Aperture Radar analyses reveal the causative fault of the 3 April 2017 Mw 6.5 Moiyabana, Botswana, earthquake. Geophysical Research Letters, 44(17), pp.8837-8846.

Mota, E.S.A., Medeiros, W.E. and Oliveira, R.G., 2020. Can Euler deconvolution outline three-dimensional magnetic sources?. Geophysical Prospecting, 68(7), pp.2271-2291.

Olea, R.A., 1974. Optimal contour mapping using universal kriging. Journal of Geophysical Research, 79(5), 695-702.

Reid, A.B.; Allsop, J.M. Granser; H., Millett, A.J., & Somerton, I.W. 1990. Magnetic interpretation in three dimensions using Euler deconvolution. Geophysics 55, 80-91.

Stavrev, P., & Reid, A. 2007. Degrees of homogeneity of potential fields and structural indices of Euler deconvolution. Geophysics 72 (1), L1-L12.

Salem, A., Williams, S., Fairhead, J. D., Smith, R., & Ravat, D. (2007). Interpretation of magnetic data using tilt-angle derivatives. Geophysics, 73(1), L1–L10.

Smith, R. S., & Salem, A. (2005). Imaging depth, structural and susceptibility from magnetic data: The advanced source parameter imaging method. Geophysics, 70(4), L31–L38.

Thompson, D.T. 1982. EULDPH: A new technique for making depth estimates from magnetic data. Geophysics 47, 31–37.

Thurston, J.B., and Smith, R.S., 1997, Automatic conversion of magnetic data to depth, dip and susceptibility contrast using the SPITM method, Geophysics, v. 62, 807-813.

Supplementary Figures

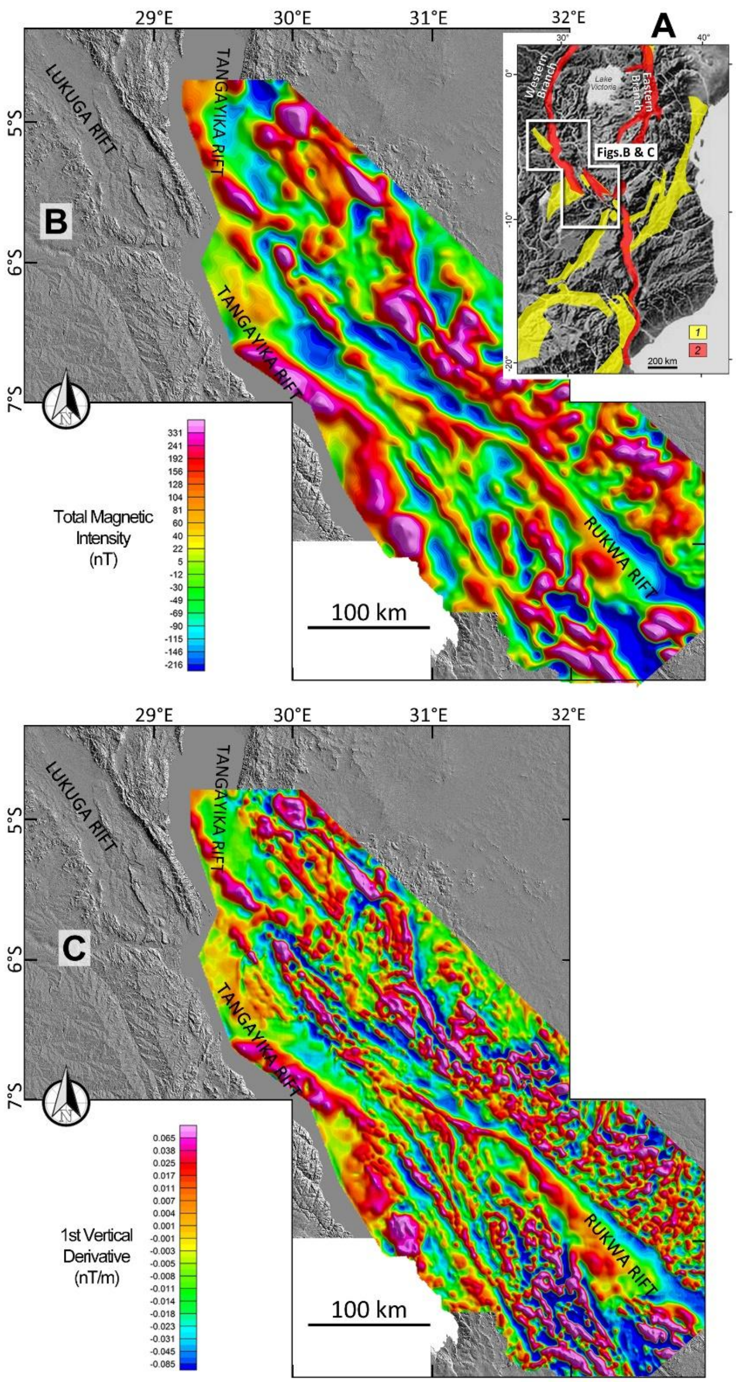

Supplementary Figure 1. A: Total Magnetic Intensity (TMI) aeromagnetic grid covering southwest Tanzania overlaid on satellite digital elevation model (DEM) hillshade map of the study area. Satellite DEM is generated from 30 m-resolution Satellite Radar Topographic Mission (SRTM) data. **B:** 1st vertical derivative of the TMI grid overlaid on satellite digital elevation model (DEM) hillshade map of the study area.

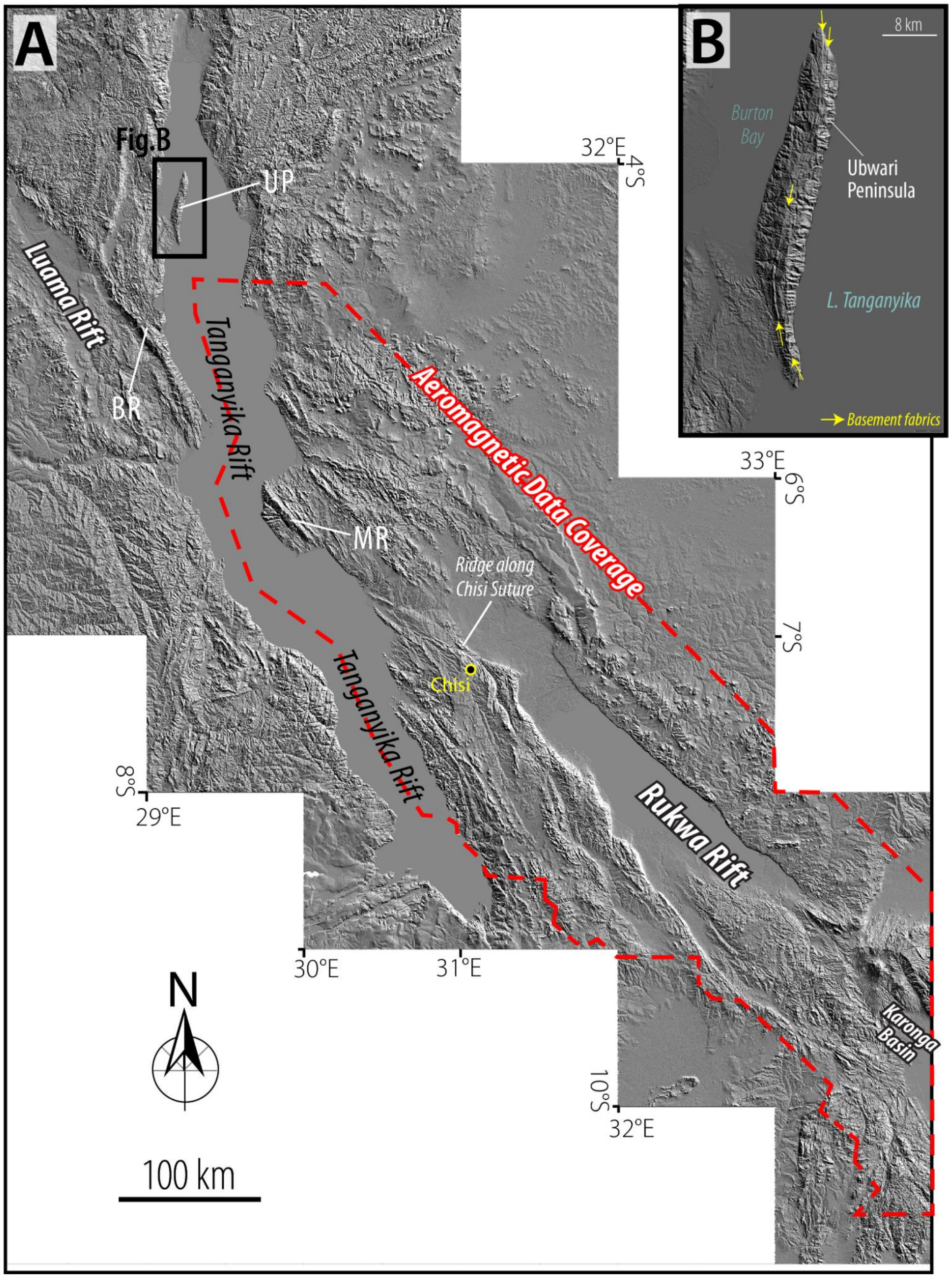

Supplementary Figure 2. A: 30 m-resolution Satellite Radar Topographic Mission (SRTM) digital elevation model (DEM) hillshade map of the study area showing the area of coverage of the aeromagnetic data shown in Figures S1A-B. Geomorphic features: BR (Busindi Ridge), UP (Ubwari Peninsula), MR (Mahale Ridge). **B:** Close-up view of the Ubwari Peninsula showing the change in the trend of the basement fabrics from a N-S trend in the north, NNE-SSW in the center, to NNW-to-NW trend in the south.

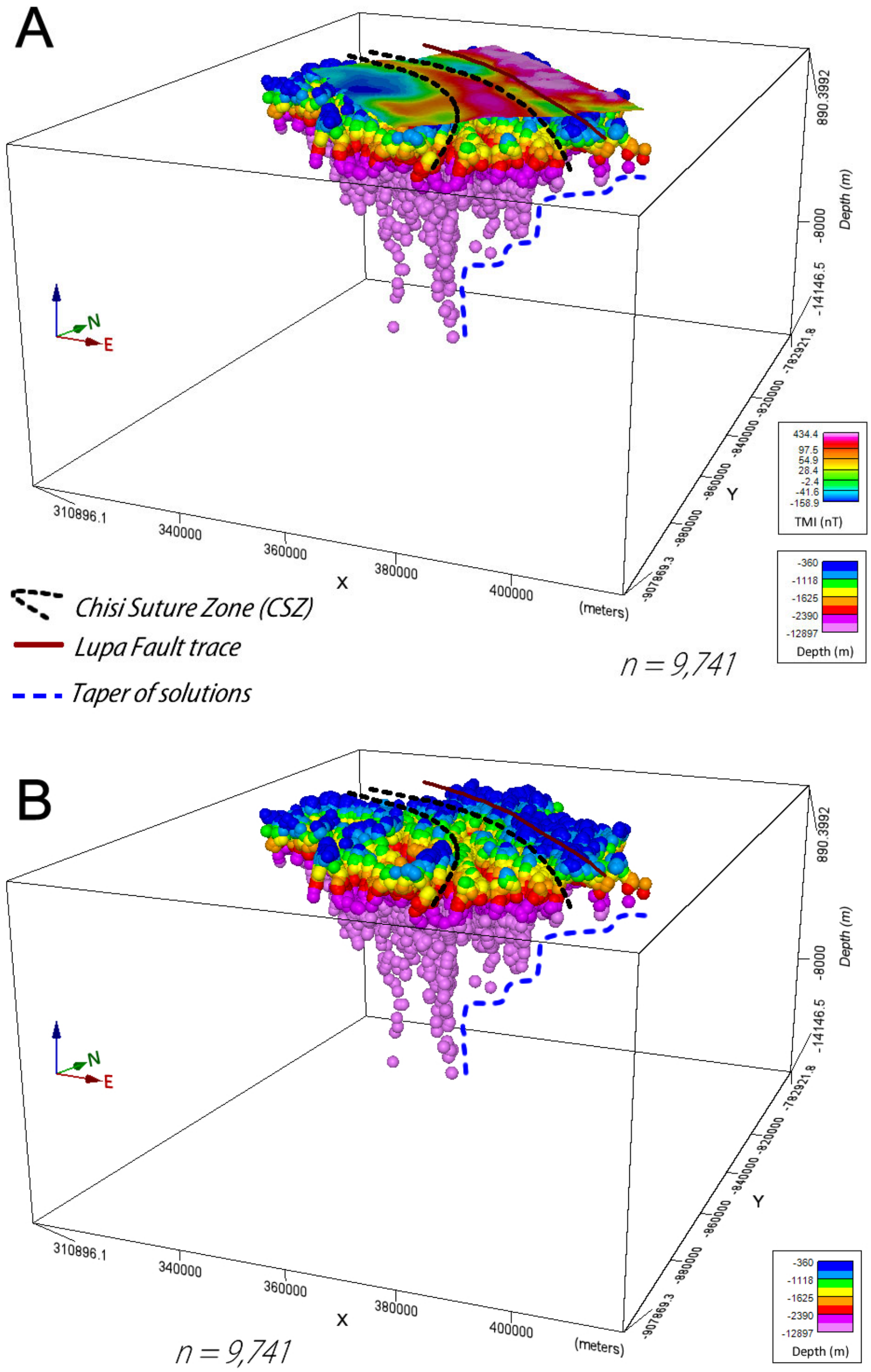

Supplementary Figure 3. A-B: Source depth solutions (colored spheres) for prominent magnetic anomalies in the Rukwa Rift, calculated from the Source Parameter Imaging (SPI) transformation of the aeromagnetic data (Fig. S1A). In Figure S3A, the 3-D plot is overlaid with the Total Magnetic Intensity Map of the Rukwa Rift. showing the Chisi Suture Zone (CSZ) magnetic lineament (bounded by dashed black line) and the Lupa Fault trace (solid brown line). The 3-D grid of the depth solutions (using the 3-D kriging technique) is shown in Figures 3B-C of the main text.

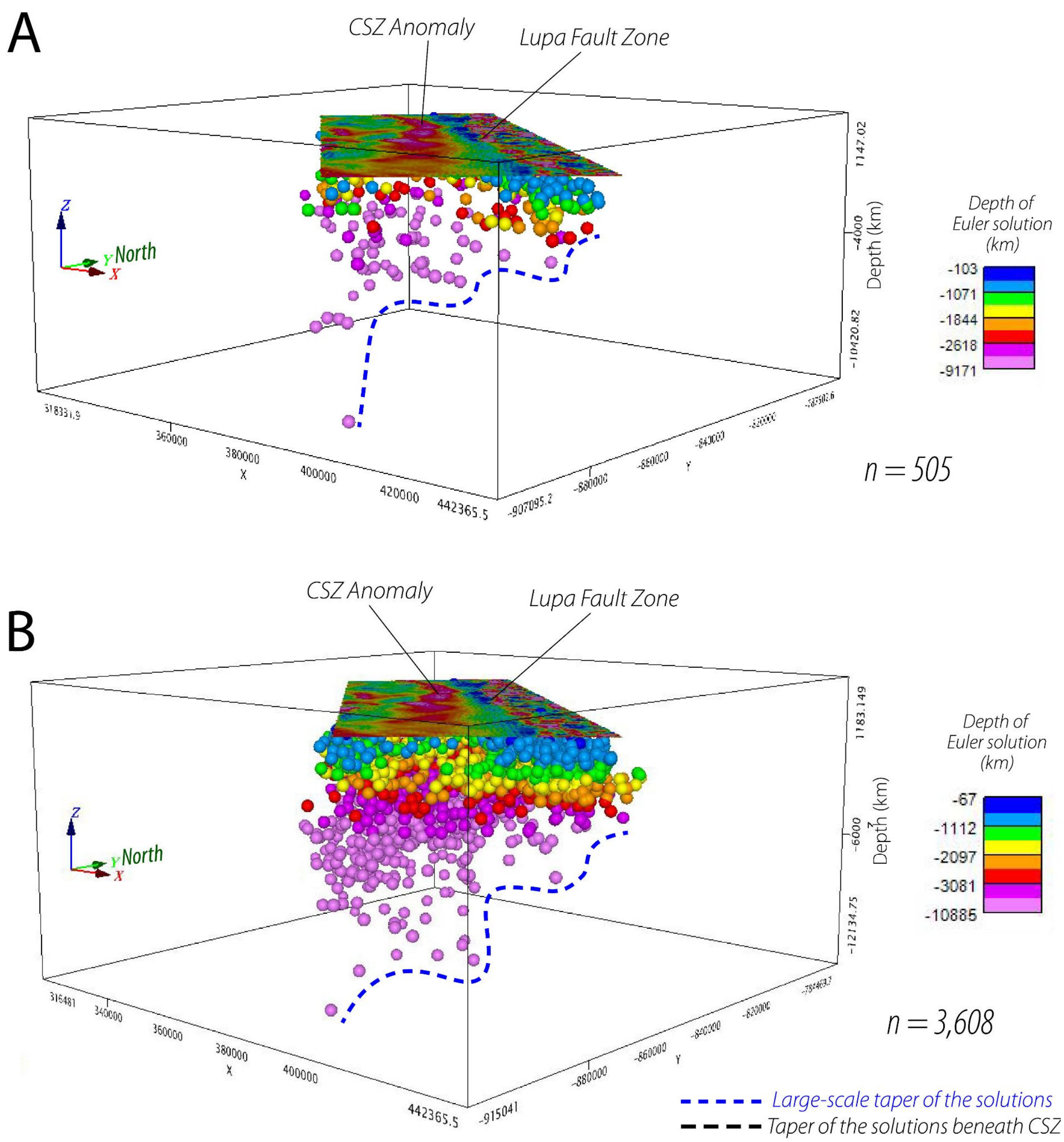

Supplementary Figure 4. A-B: Source depth solutions (colored spheres) of prominent magnetic anomalies in the Rukwa Rift, calculated from the Euler Deconvolution of the magnetic data. Figure S4A is a minimum solution, obtained by a 5% maximum depth tolerance and window size of 3; whereas Figure S4B is a maximum solution, obtained by a 10% maximum depth tolerance and window size of 5. CSZ = Chisi Suture Zone.